Received: 3 May 2017 | Revised: 12 July 2017 | Accepted: 14 July 2017

DOI: 10.1111/pce.13040

WILEY Plant, Cell & Environment

ORIGINAL ARTICLE

Components of mesophyll resistance and their environmental responses: A theoretical modelling analysis

Yi Xiao[1] | Xin-Guang Zhu[1,2]

[1] Institute of Plant Physiology & Ecology, Shanghai Institutes for Biological Sciences, Chinese Academy of Sciences, Shanghai, China

[2] State Key Laboratory of Hybrid Rice, Hunan Hybrid Rice Research Center, Changsha, China

Correspondence
Xin-Guang Zhu, Institute of Plant Physiology and Ecology, Shanghai Institutes for Biological Sciences, Chinese Academy of Sciences, Shanghai 200032, China.
Email: zhuxg@sippe.ac.cn

Funding information
Bill and Melinda Gates Foundation, Grant/Award Number: OPP1129902, OPP1060461 and OPP1014417; Chinese Academy of Sciences, Grant/Award Number: XDA08020301; National Science Foundation of China, Grant/Award Number: 30970213; Ministry of Science and Technology of China, Grant/Award Number: 2011DFA and 2015CB150104

Abstract

Mesophyll resistance (r_m), stomatal resistance, and biochemical limitations are recognized as three critical factors limiting leaf photosynthesis. Contrary to the expectation of being a constant, r_m not only varies with light and CO_2 conditions but also shows different responses among species. To elucidate the mechanistic basis of these responses, we derived an analytical model of r_m, which incorporates various anatomical and biochemical factors including permeabilities of cell wall and chloroplast envelope to CO_2 and HCO_3^-, carbonic anhydrase activities in cytosol and stroma, Rubisco activities, and relative location of mitochondria and chloroplast. The robustness of this model was confirmed by comparing the predicted r_m and its components to numerical models developed at cell and leaf levels, which incorporate detailed 3-dimensional cell and leaf anatomies, CO_2 hydration and diffusion processes from intercellular air space to stroma, and CO_2 fixation by Rubisco. A combination of these model analyses shows that the varying r_m is influenced by four biochemical factors: (a) nonuniform photosynthesis status across the leaf, (b) photorespiration and respiration, (c) bicarbonate leakage on the chloroplast envelope, and (d) hydration activity in cytosol and stroma. This study provides a theoretical framework to study components of r_m and their responses to environmental perturbations.

KEYWORDS

analytical model, mesophyll resistance, mitochondria position, reaction–diffusion model

1 | INTRODUCTION

Mesophyll resistance (r_m) represents a series of physical barriers and biochemical components residing in the cell wall, cytosol, chloroplast envelope, and stroma, which limits CO_2 diffusion and causes a gradient of CO_2 from the substomatal cavity (C_i) to the carboxylation site in the chloroplast (C_c). Mesophyll resistance (r_m) equals the gradient C_i–C_c divided by the flux of net photosynthesis (A_N), which is defined analogous to resistance in Ohm's law for electricity (Evans, Kaldenhoff, Genty, & Terashima, 2009). It is worth noticing that the definition of r_m implicitly assumes that a leaf can be averaged to one cell at a certain middle position of the leaf, ignoring the complexity of the leaf structure (Parkhurst, 1994). Recently, r_m is found to be an important limiting factor to leaf photosynthesis in many species in addition to the limitation of stomatal resistance and biochemical process (Flexas et al., 2012; Griffiths & Helliker, 2013). Improving mesophyll conductance (g_m), which is the reciprocal of r_m, is also regarded as an ideal option to increase water use efficiency of crops (Zhu, Long, & Ort, 2010; Flexas et al., 2012).

Two classic methods are commonly used to measure instantaneous r_m. One is the variable J (electron transport rate) method, in which gas exchange and chlorophyll fluorescence signals are measured simultaneously. The other is the stable carbon isotope discrimination ($\Delta^{13}C$) method, in which gas exchange and ^{13}C discrimination of leaf photosynthesis are measured simultaneously (Harley, Loreto, Di Marco, & Sharkey, 1992). With the variable J method, a number of studies reported a varying r_m with increase of C_i, and the patterns are surprisingly similar; that is, g_m appears to first increase and then decrease gradually with the increase of C_i (Flexas et al., 2007; Hassiotou, Ludwig, Renton, Veneklaas, & Evans, 2009; Vrábl, Vašková, Hronková, Flexas, & Šantrček, 2009; Xiong et al., 2015). In addition to the CO_2 response, g_m is also reported to decrease with the increase of irradiance in several species (Flexas et al., 2012; Xiong et al., 2015). Recent work by Théroux-Rancourt and Gilbert (2017) combines the variable J method with a multilayer leaf model and shows g_m is an emergent property of the leaf structure, whereas, with the $\Delta^{13}C$ method, a similar CO_2 and light response of r_m is observed by Flexas et al. (2007) and Vrábl et al. (2009). But r_m is also reported to show no response to C_i and light

under low oxygen concentrations in wheat (Tazoe, von Caemmerer, Badger, & Evans, 2009). However, Tazoe et al. (2011) also observed that g_m decreases with CO_2 under 2% O_2 and has a less sensitive response under 21% O_2. Significant short-term responses to both light and CO_2 were observed by Douthe, Dreyer, Brendel, and Warren (2012) and Douthe, Dreyer, Epron, and Warren (2011).

Various mechanisms were proposed to explain the CO_2 and light dependency of r_m. In the measurement with either variable J method or $\Delta^{13}C$ method, a biased estimate of parameters such as the day respiration (R_d) and chloroplastic CO_2 compensation point (Γ^*) may influence the estimated r_m (Harley et al., 1992; L. Gu & Sun, 2014; Pons et al., 2009). Current chlorophyll fluorescence measurement technologies potentially underestimate the photosynthetic electron transport rate (J; Loriaux et al., 2013), which may also affect the measured dependency of r_m on CO_2 and light via the variable J method (Evans, 2009; L. Gu & Sun, 2014). In the $\Delta^{13}C$ method, different formulas of carbon isotope discrimination (Evans & von Caemmerer, 2013; Farquhar & Cernusak, 2012; L. Gu & Sun, 2014), in particular with either a constant or variable fractionation factor associated with photorespiration (f), can lead to different estimates of r_m (Evans & von Caemmerer, 2013; Griffiths & Helliker, 2013; Tholen et al., 2012).

Mathematical models, in particular analytical models, provide an alternative and more intuitive approach to study r_m and its environmental responses. A three-dimensional (3D) reaction–diffusion (R-D) model of a single mesophyll cell (MSC) has been developed to study mechanisms underlying the varying r_m (Tholen & Zhu, 2011). On the basis of that 3D model, an analytical model of r_m is derived, which incorporates the impacts of photorespiratory and respiratory fluxes (Tholen, Éthier, & Genty, 2014; Tholen et al., 2012; Tholen & Zhu, 2011). There are also other studies developing analytical models of r_m since decades ago, which link r_m and its components to measured anatomical features in different species (Berghuijs et al., 2015; Evans et al., 2009; Nobel, 1999; Peguero-Pina et al., 2012; Tomás et al., 2013; Tosens & Niinemets, 2012; Tosens, Niinemets, Westoby, & Wright, 2012) and quantify the contribution of the cell wall, cytosol, chloroplast envelope, and stroma to the measured r_m. In these studies, parameters such as thickness of the cell wall, cytosol, and chloroplast were estimated from light microscopy and transmission electron microscopy images, whereas parameters such as wall porosity, membrane permeability, diffusion viscosity, and effective path length of CO_2 diffusion were either assumed or fitted from data collected from a group of species (Berghuijs et al., 2015; Tomás et al., 2013), which can potentially lead to overparameterization. In all these efforts of developing analytical models of r_m, the detailed biochemical components and the associated 3D nature of CO_2 and bicarbonate diffusion in an MSC or leaf are simplified. This simplification prevents using such models in studying components of r_m and their responses under different environments.

In addition to being a major tool in studying mechanisms of mesophyll resistance (Tholen & Zhu, 2011), 3D mechanistic models of mesophyll resistance can be used as a supporting tool to guide development of analytical models. Using such mechanistic 3D R-D models, we not only can test the influence of different biochemical and biophysical parameters such as dark respiration (R_d), Γ^*, wall porosity, membrane permeability, and diffusion viscosity on r_m but also can predict the ground truth of the responses of r_m to different light and CO_2 conditions.

In this paper, to facilitate our understanding of the r_m of rice, which is one of the most important food for the world, we derived a new analytical model of r_m, which includes all known anatomical and biochemical factors influencing r_m. We validated the robustness of the model by comparing its prediction with 3D R-D models at both the mesophyll and leaf levels. With these theoretical frameworks, we systematically evaluated the magnitude and responses of r_m under different light and CO_2 conditions. Finally, we discuss potential errors in using this new analytical model in studying r_m in the laboratory.

2 | THEORY AND METHODS

2.1 | An analytical model of mesophyll resistance

Mesophyll resistance represents the total resistance of CO_2 diffusion from the substomatal cavity to chloroplast stroma (Figure 1a). Mesophyll resistance (r_m) is divided into a gaseous phase (r_{ias}) and a liquid phase (r_{liq}). CO_2 first diffuses through intercellular air space, with CO_2 concentration ($[CO_2]$) decrease from gas-phase $[CO_2]$ C_i in the substomatal cavity to liquid-phase $[CO_2]$ C_{w_o}, that is, $[CO_2]$ at the outer surface of the cell wall. Throughout the text, the unit of $[CO_2]$ is bars, and the unit of all resistance is per mole per square metre second bar. It is important to note that an ideal gas equation and Henry's law are applied respectively to convert the unit of $[CO_2]$ in gaseous and liquid phases. Therefore, r_m is calculated as a composite resistance of gaseous and liquid components as (Niinemets & Reichstein, 2003; Tomás et al., 2013)

$$r_m = r_{ias}\frac{RT}{H_c} + r_{liq} = \frac{C_i' - C_{w\_o}}{A_N} + \frac{C_{w\_o} - C_c}{A_N}, \quad (1)$$

where H_c is the Henry law constant (bar m^3 mol^{-1}) for CO_2, R is the gas constant (bar m^3 K^{-1} mol^{-1}), and T is the absolute temperature (K; Niinemets & Reichstein, 2003; Tomás et al., 2013). A dimensionless factor $(RT)/H_c$ is needed to convert r_{ias} to its corresponding liquid-phase equivalent resistance. In terms of CO_2, this is equivalent to replacing the gas-phase C_i with its equivalent liquid-phase $C_i' = C_i \cdot (RT)/H_c$ (Niinemets & Reichstein, 2003; Tomás et al., 2013).

The gas-phase resistance is modelled the same as (Tomás et al., 2013)

$$r_{ias} = \frac{\Delta L_{ias} \cdot \varsigma}{D_a \cdot f_{ias}}, \quad (2)$$

where ΔL_{ias} (m) is the average gas-phase thickness, which is taken as half of the mesophyll thickness here; ς (m m^{-1}) is the tortuosity of the diffusion path, suggested to be 1.57 (Niinemets & Reichstein, 2003; Tomás et al., 2013); D_a (m^2 s^{-1}) is the diffusion coefficient of CO_2 in the gas phase; and f_{ias} is the fraction of leaf intercellular air space.

In the liquid phase of diffusion, CO_2 first diffuses through the cell wall and membrane, during which $[CO_2]$ decreases from C_{w_o} to C_{w_i}, that is, $[CO_2]$ at the inner surface of the cell wall. Next, CO_2 diffuses through the cytosol to reach the surface of the chloroplast envelope, with the $[CO_2]$ further decreasing to C_{se_o}, that is, $[CO_2]$ at the outer surface of the chloroplast envelope facing the cell wall. Then the chloroplast envelope forms another barrier, where $[CO_2]$ further decreases to C_{se_i}, that is, $[CO_2]$ at the inner surface of the chloroplast

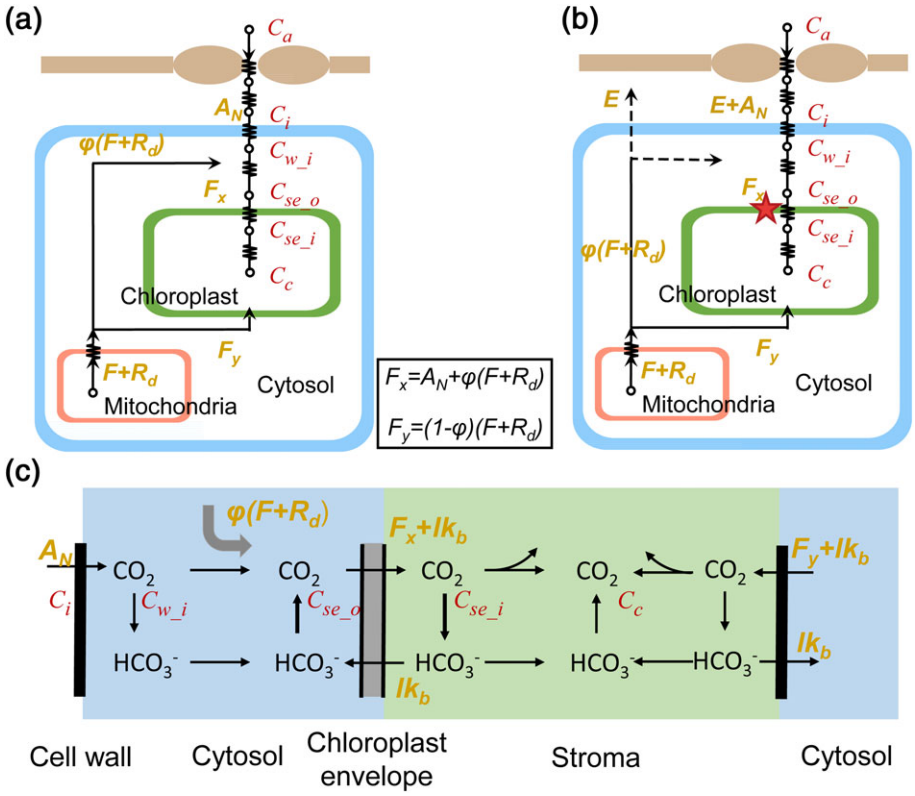

FIGURE 1 (a) The schema of CO_2 reaction and diffusion processes inside a cell incorporated by our new biochemical–biophysical–anatomical formula of mesophyll resistance. The influence of the relative location between mitochondria and chloroplasts was represented by a fractionation factor φ. (b) Leakage of CO_2 from the mesophyll cell to the air space (flux E) does not influence the calculation of defined resistance of each barrier. (c) One-dimensional representation of the four CO_2 diffusion barriers inside the cell and corresponding boundary flux

envelope. Finally, CO_2 diffuses inside the chloroplast stroma and is fixed by Rubisco, resulting in C_c, that is, the average $[CO_2]$ in the stroma (Figure 1a, extended based on Tholen et al., 2012).

In Figure 1a, the photorespired and respired CO_2 from mitochondria ($F + R_d$) are separated into two fluxes with different diffusion paths and further refixed by Rubisco, which has been reported to be influenced by the relative position of mitochondria and chloroplast (Busch et al., 2013). Although in Figure 1a, all the (photo)respired flux $F + R_d$ finally enters the chloroplast, in a real leaf, part of $F + R_d$ can leak to the air (Figure 1b), which can be detected by isotope signals. However, there is no difference in the calculation of all resistances between the frameworks of Figure 1a,b because resistance merely relies on net flux across the membrane.

The r_{liq} therefore is mathematically divided into four items corresponding to different barriers (Equation 3), including resistance of the cell wall and membrane (r_{I_wall}), resistance of the cytosol between chloroplast and the cell wall (r_{II_cyto}), resistance of the chloroplast envelope (r_{III_se}), and resistance of the stroma (r_{IV_chlo}), that is,

$$r_{liq}=\frac{C_{w\_o}-C_c}{A_N}=\frac{C_{w\_o}-C_{w\_i}}{A_N}+\frac{C_{w\_i}-C_{se\_o}}{A_N}+\frac{C_{se\_o}-C_{se\_i}}{A_N}+\frac{C_{se\_i}-C_c}{A_N}$$
$$=r_{I\_wall}+r_{II\_cyto}+r_{III\_se}+r_{IV\_chlo}, \quad (3)$$

where A_N is the net photosynthesis rate per leaf area. On the basis of this partitioning, a one-dimensional (1D) approximation of the R-D processes of these four barriers is presented in Figure 1c and used as the basis to derive an analytical model.

2.2 | Resistance of the cell wall and plasma membrane

The resistance of the cell wall and membrane (r_{I_wall}) is defined as the difference of $[CO_2]$ on two sides of the barrier divided by A_N (Equation 4). Because we assume that there are no other fluxes across this barrier influencing the CO_2 gradient C_{w_o}–C_{w_i} (Figure 1c), it is expected that the r_{I_wall} is equal to the physical resistance of the cell wall and plasma membrane (Equation 4, Tomás et al., 2013).

$$r_{I\_wall}=\frac{C_{w\_o}-C_{w\_i}}{A_N}=S_m\frac{d_w}{D_c\cdot r_{f,w}\cdot p}, \quad (4)$$

where S_m (m^2) is the area of cell wall that is exposed to the intercellular air space per leaf area. The scale factor S_m here is introduced due to the increase in area available for CO_2 diffusion. The thickness of cell wall is denoted by d_w (m), the aqueous phase diffusion coefficient of CO_2 by D_c ($m^2\ s^{-1}$), the decrease of diffusion coefficient compared to free diffusion in water by $r_{f,w}$, and the effective porosity of the membrane by p (Evans et al., 2009; Tomás et al., 2013).

2.3 | Resistance of cytosol

Resistance of the cytosol (r_{II_cyto}) is defined as the gradient of $[CO_2]$ between the inner cell wall (C_{w_i}) and the outer surface of the chloroplast envelope (C_{se_o}) divided by A_N. Inside the cytosol, there are three sources of CO_2: (a) CO_2 from the intercellular air space, (b) CO_2 generated from dehydration of HCO_3^-, and (c) CO_2 released from

mitochondria by photorespiration and respiration. These three sources of CO_2 together form the CO_2 gradient in the cytosol and determine the CO_2 diffusion flux across the cytosol (Figure 1c). In our approximation, the influence of the (photo)respiratory flux in the cytosol is not considered for simplicity. In other words, only the effect of CO_2 diffusion and the process of hydration are included in the 1D approximation.

The expression of r_{II_cyto} is then derived and simplified as the sum of two parts (Equation 5, see Appendix S2 for derivations in detail).

$$r_{II\_cyto} = \frac{C_{w\_i} - C_{se\_o}}{A_N} = r_{II\_cyto\_CAfree} + r_{II\_cyto\_CA}. \quad (5)$$

The first part matches the formula by Evans et al. (2009; Equation 6), where they calculated the resistance of the cytosol, assuming there is no limitation of carbonic anhydrase (CA). We designated this item to be $r_{II\_cyto\_CAfree}$. Here, S_c ($m^2\ m^{-2}$) is the area of chloroplast exposed to the intercellular air space. The scale factor S_c here actually represents the area of parallel 1D diffusion in a 3D leaf from the outer cell wall to the chloroplast (Evans et al., 2009; Tomás et al., 2013). The thickness of the cytosol between the chloroplast and cell wall is represented by d_c (m); $D_{c,c}$ and $D_{b,c}$ represent $D_c \times r_{f,c}$ and $D_b \times r_{f,c}$, respectively, meaning the effective diffusion coefficients of CO_2 and HCO_3^- in the cytosol; K_{eq} (mol m^{-3}) is the equilibrium constant; and H (mol m^{-3}) is the proton concentration.

$$r_{II\_cyto\_CAfree} = S_c \frac{d_c}{D_{c,c} + D_{b,c}\frac{K_{eq}}{H}}. \quad (6)$$

Furthermore, our calculation shows that the limitation from hydration catalysed by CA actually formed another item, which we denote as $r_{II\_cyto\_CA}$:

$$r_{II\_cyto\_CA} = S_c \alpha \left(D_{c,c}\frac{lk_b}{A_N} + D_{b,c}\frac{K_{eq}}{H}\left(2 + \frac{lk_b}{A_N}\right)\right), \quad (7)$$

where α is a function of $D_{c,c}$, $D_{b,c}$, and biochemical constants of the hydration reaction (see Appendix S2 for the expression in detail). The leakage rate of HCO_3^- from the chloroplast to the cytosol per leaf area is denoted by lk_b (mol $m^{-2}\ s^{-1}$). It is worth noticing that under different light and CO_2 conditions, the expression of r_{II_cyto} solved is simplified to be independent of the input parameter C_{w_i}. It becomes merely a function of the ratio lk_b/A_N in addition to physical parameters of diffusion and biochemical parameters of hydration (Equations 6 and 7).

2.4 | Resistance of the chloroplast envelope

The effect of relative position between the chloroplast and mitochondria is represented by a parameter φ (Figure 1). That is, a portion of the (photo)respiratory flux, $\varphi(F + R_d)$, influences the CO_2 gradient between the cell wall and chloroplast envelope, which will increase the net flux across the chloroplast envelope facing the cell wall from A_N to $F_x = A_N + \varphi(F + R_d)$; see Figure 1a,b. The rest of the (photo)respiratory flux $F_y = (1 - \varphi)(F + R_d)$ diffuses through the abaxial side of chloroplast.

Notice that, on the chloroplast envelope, there is an efflux in the form of HCO_3^- (lk_b) due to the difference of pH values between the cytosol and stroma. The influx of carbon in the form of CO_2 should equal $F_x + lk_b$ following the mass conservation of carbon (Figure 1c). For the derivation of r_{III_se} (Equation 8), CO_2 diffusion through the envelope is treated as two resistances in parallel. In one of the fluxes, CO_2 directly diffuses through the envelope. In another flux, CO_2 is first hydrated to HCO_3^- and diffuses through the envelope and enters the stroma where HCO_3^- is dehydrated back to CO_2. F_x was naturally introduced to the numerator and denominator considering that the real flux corresponding to the CO_2 gradient $C_{se\_o} - C_{se\_i}$ across the chloroplast envelope is F_x rather than A.

$$r_{III\_se} = \frac{C_{se\_o} - C_{se\_i}}{F_x}\frac{F_x}{A_N} = r_{se\_c} S_c \frac{1}{1 - \frac{lk_b}{F_x + lk_b}}\frac{F_x}{A_N} \quad (8)$$

Here, r_{se_c} is the resistance of the chloroplast envelope for CO_2.

2.5 | Resistance of the chloroplast stroma

R-D processes in the stroma are similar to those in the cytosol except the additional carboxylation of CO_2 (Figure 1c, and see Equations S12 and S18 in Appendix S2). Similar to the case for the chloroplast envelope, the flux corresponding to the CO_2 gradient $C_{se\_i} - C_c$ should be F_x (Figure 1c), so the expression of r_{IV_chlo} is written and solved as

$$r_{IV\_chlo} = \frac{C_{se\_i} - C_c}{F_x}\frac{F_x}{A_N} = S_c \left(\frac{d_s}{D_{c,s} + D_{b,s}\frac{K_{eq}}{H}}\frac{2V_c - 3F_y}{6A_N} + \beta \right), \quad (9)$$

where $D_{c,s}$ and $D_{b,s}$ equal $D_c \times r_{f,s}$ and $D_b \times r_{f,s}$, respectively, representing the effective diffusion coefficients of CO_2 and HCO_3^- in the stroma, d_s (m) is the thickness of the chloroplast, V_c (mol $m^{-2}\ s^{-1}$) is the carboxylation rate per leaf area, and β is a complex function of constants of diffusion, hydration, and carboxylation processes (see Appendix S2 for expressions and derivations in detail).

Finally, by combining these different components of r_{liq} (Equations 4, 5, 8, and 9), we derive a complete formula for r_{liq}. Further combining this expression of r_{liq} with r_{ias} (Equations 1 and 2), we obtain an analytical model of the whole r_m.

3 | A THREE-DIMENSIONAL REACTION–DIFFUSION MODEL OF MESOPHYLL CELL RESISTANCE

We follow the procedure of Tholen and Zhu (2011) to develop a 3D R-D model of mesophyll resistance. In this model, rice MSC is simplified to be a flower-shaped object in 3D (Figure 2b), with the intention of mimicking lobes in rice, which enhance the absorption of light and CO_2 due to an increased cell surface to volume ratio (Sage & Sage, 2009). Inside each MSC, chloroplasts are simplified to be a layer next to the cell wall, and next to the chloroplast layer, one mitochondrion is distributed inside each lobe (Figure 2). The thickness of the chloroplast layer is assumed to be 2 μm, resulting in a volume percentage of chloroplasts being about 59% of the total cell volume (Sage & Sage, 2009).

To test the effect of φ on r_m in the analytical formula, four different cell structures that have different relative positions of mitochondrion to chloroplast were constructed; therefore, φ will be different in these structures. Only a quarter of these cell structures are modelled and shown in Figure 3 because the shapes are symmetrical. On the basis of the cell anatomy in Figure 2b, holes are made on the chloroplast layer to mimic gaps between the chloroplasts in a real leaf (Figure 3a). Then mitochondria are generally moved closer to the cell wall (Figure 3b,c). In addition, another kind of cell anatomy is

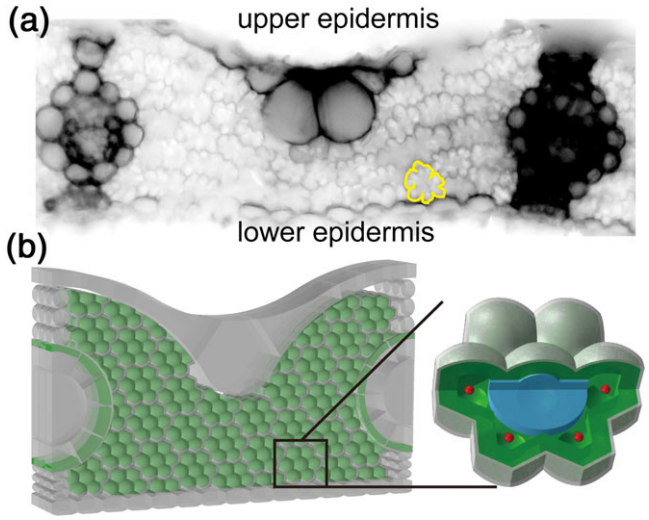

FIGURE 2 (a) Illustration of a transverse cross-sectional image of a rice leaf segment. Flower-shaped mesophyll cells (MSCs) are compact with each other in the section. (b) Illustration of the reconstructed rice leaf anatomy with epidermis cells, MSCs, bundle sheath cells, veins, and bundle sheath extension cells. Within mesophyll cells, the green region represents chloroplasts, red balls represent mitochondria, and the blue region represents vacuole. In each transverse layer, MSCs are in contact with each other, and between two transverse layers, the surface of MSCs are in contact with the intercellular air space

constructed, in which holes on the chloroplast membrane are located apart from the position of mitochondria (Figure 3d). The surface area of the chloroplast layer is kept the same for all these structures in Figure 3, and gaps made here cover about 3.4% of the MSC surface.

4 | A THREE-DIMENSIONAL REACTION–DIFFUSION MODEL OF A RICE LEAF

We further developed an integrated 3D model of leaf photosynthesis where internal light environment, CO_2 profiles, and biochemical processes were explicitly simulated. The integrated model is an extension of the cell-level R-D model (Tholen & Zhu, 2011) using a reconstructed 3D anatomy of a rice leaf. To do this, first, the number of MSCs between two veins and the number of layers of MSCs between leaf adaxial and abaxial surfaces are estimated from transverse section images of rice leaves (Figure 2a). Then with the leaf thickness and vein distance estimated from the same images, the length and width of the MSC are calculated. Meanwhile, from the rice longitudinal cross section, the thickness of MSC can be estimated. In addition to MSCs, the shape and size of other cells such as upper epidermis, bulliform cells, lower epidermis, veins, bundle sheath cells, and bundle sheath extension cells are also reconstructed based on rice leaf cross-sectional images (Figure 2). All parameters used for reconstructing the geometry in Figure 2b are listed in Supporting Information Table **S1**. It is worth mentioning that in our modelled 3D leaf, the MSCs are compact and contact with each other in each transverse layer (Figure 2b), whereas between two transverse layers, the surface of MSCs is in contact with intercellular air space. Chlorophyll concentration is assumed to be the same in all chloroplasts in MSCs and bundle sheath cells, and the total chlorophyll content per leaf area for the model is 76 μg cm^{-2}.

With this reconstructed 3D leaf anatomy, the internal light environment is simulated by a ray tracing algorithm (Xiao et al., 2016), which predicts the light absorption of the chloroplast membrane inside each cell (Supporting Information Figure S1). The predicted leaf internal light environment is then integrated with the CO_2 R-D model of individual MSCs. Specifically, light absorbed by the chloroplast of individual MSCs affects the potential electron transport rate *J*, which further influences the photosynthetic CO_2 uptake rate by limiting the ribulose 1,5-bisphosphate regeneration rate (refer to Appendix **S1** for details).

5 | PARAMETERIZATION AND PREDICTION OF THE THREE-DIMENSIONAL MODELS

The full list of parameters used in the 3D MSC model and 3D leaf model is detailed in Table 1. Among these, parameters related to CA-catalysed reactions and CO_2 diffusion through different cellular components follow Tholen and Zhu (2011). The Rubisco-limited maximal carboxylation rate and maximal electron transport rate for the

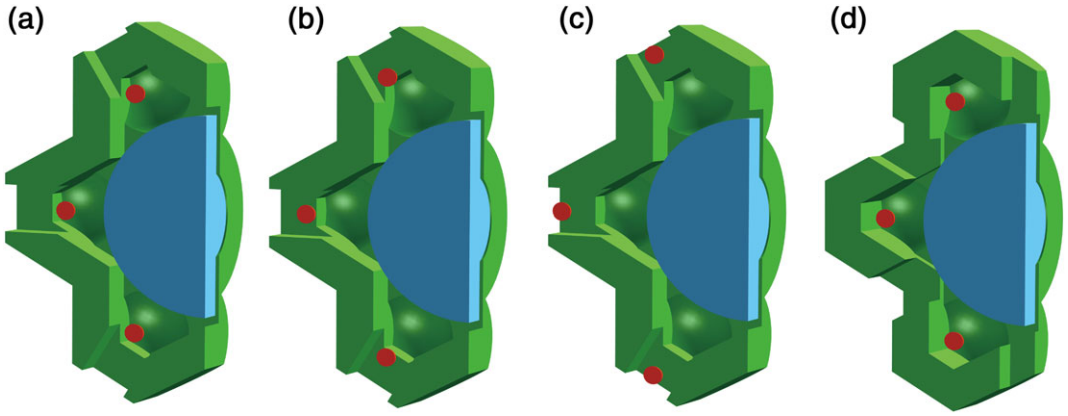

FIGURE 3 Cell anatomies with different relative positions of mitochondria and chloroplast. A quarter of cell structure was modelled and shown here. On the basis of the cell anatomy in Figure 2b, holes are made on the chloroplast layer either above the position of mitochondria (a–c) or apart from the position of mitochondria (d). Different distances between mitochondria and cell wall were made in Panels a–c

whole leaf are assigned as 115 and 216 μmol m^{-2} s^{-1}, representing photosynthetic properties of a typical sunlit rice leaf (J. Gu, Yin, Stomph, Wang, & Struik, 2012). In this study, as a simplification, we assume that the V_{cmax} and J_{max} are equally distributed into different MSCs. The 3D R-D models are implemented and solved using the finite element method (COMSOL Multiphysics 4.3, Stockholm, Sweden). The output of the model simulation is a spatial distribution of concentrations of CO_2 and HCO_3^- and corresponding fluxes. C_c is calculated as a volume average of [CO_2] in the stroma. Concentrations such as C_{w_o}, C_{w_i}, C_{se_o}, and C_{se_i} are calculated as the surface average of [CO_2] on the corresponding outer or inner surface. Fluxes such as A_N, F, R_d, and lk_b are calculated as surface integration on corresponding surfaces. Further, for the 3D cell model, A_N is calculated as the predicted photosynthesis rate per cell surface area multiplied by S_m estimated from the 3D leaf model. The ratio between the CO_2 gradient $C_{w\_o}-C_c$ and A_N is r_{liq}. The resistance of each barrier is then calculated as the ratio between the [CO_2] gradient across that barrier and A_N, whereas, with the 3D leaf model, we estimate the total r_m as the ratio between $[C_i \cdot (RT)/H - C_c]$ and A_N (Equation 1).

6 | PARAMETERIZATION AND VALIDATION OF THE ANALYTICAL MODEL

Parameters used in the analytical models are either input for the 3D R-D models, for example, pH of the cytosol or stroma and concentrations of CA, or output from the 3D R-D models, for example, A_N, photorespiratory flux (F), and the leakage of HCO_3^- from chloroplast to cytosol (lk_b; Table 1). Such a treatment enables direct comparison between the analytical model and 3D R-D models. The parameter φ was set to be 0, considering that the coverage of the surface area of the MSC wall by the chloroplast was 100% in the rice cell modelled.

To validate the performance of the analytical solution, we calculated r_m and its components using the analytical model for different light and CO_2 conditions. Similarly, we modelled and estimated r_m and its components using 3D R-D models at both the cell and leaf levels.

7 | RESULTS

7.1 | Comparison between mesophyll resistance of the liquid phase predicted by the analytical model and three-dimensional cell model

On the basis of the mathematical decomposition of mesophyll resistance (r_m; Equations 1 and 3), r_m is divided into resistance of the gaseous phase (r_{ias}) and resistance of the liquid phase (r_{liq}), whereas r_{liq} is divided into four components, namely, resistance of the cell wall and membrane (r_{I_wall}), resistance of the cytosol (r_{II_cyto}), resistance of the chloroplast envelope (r_{III_se}), and resistance of the interior stroma (r_{IV_chlo}). Here, a new analytical model of r_{liq} is derived by using explicit formulas for each of these four barriers (Table 1, Spreadsheet **S1**). The outputs of this analytical model are r_{liq} and its components. Its input

TABLE 1 Variables and constants used in the new analytical model and three-dimensional reaction–diffusion models on the cell level and leaf level

Parameters		Name	Symbol	Value	Units	Components
Parameters used in analytical model	Biophysical and anatomical parameters	Cell wall thickness	d_w	1.5×10^{-7}	m	I
		Effective porosity of the cell wall	p	0.15	unitless	I
		Liquid-phase CO_2 diffusion coefficient	D_c	1.83×10^{-9}	m^2 s^{-1}	II, IV
		HCO_3^- diffusion coefficient	D_b	$0.52 \times D_c$	m^2 s^{-1}	II, IV
		Cytosol viscosity	$r_{f,c}$	0.5	unitless	II
		Stroma viscosity	$r_{f,s}$	0.1	unitless	IV
		Thickness of cytosol between the cell wall and chloroplast	d_c	Input	m	II
		Thickness of the chloroplast	d_s	Input	m	IV
	Biochemical parameters	Carbonic anhydrase (CA) turnover rate	k_a	3×10^5	s^{-1}	II, IV
		CA concentration cytosol	$X_{a,c}$	$0.5 \times X_{a,s}$	mol m^{-3}	II
		CA concentration stroma	$X_{a,s}$	0.27	mol m^{-3}	IV
		Proton concentration	H	10^{-pH}	mol m^{-3}	II, IV
		Cytosol pH	pH_c	7.3	unitless	II
		Chloroplast pH	pH_s	8	unitless	IV
		CA equilibrium constant	K_{eq}	5.6×10^{-7}	mol m^{-3}	II, IV
		CA hydration K_m	K_a	1.5	mol m^{-3}	II, IV
		CA dehydration K_m	K_{HCO3}	34	mol m^{-3}	II, IV
	Other variables	[CO_2] in intercellular airspace	C_i	Input	mol m^{-3}	IV
		Net photosynthesis rate	A_N	Input	mol m^{-2} s^{-1}	II, III, IV
		HCO_3^- leakage	lk_b	Input	mol m^{-2} s^{-1}	II, III, IV
		Photorespiration rate	F	Input	mol m^{-2} s^{-1}	III, IV
		Respiration rate	R_d	Input	mol m^{-2} s^{-1}	III, IV
		Mitochondria position related effect on r_m	φ	Input	unitless	III, IV
Additional parameters used in the three-dimensional model		Maximal Rubisco carboxylation rate	V_{cmax}	115	mol m^{-2} s^{-1}	
		Maximal electron transport rate	J_{max}	216	mol m^{-2} s^{-1}	
		Convexity index	θ	0.98	unitless	
		Fraction of absorbed photons which do not drive electron generation	f	0.15	unitless	

parameters for this model include (a) biophysical parameters such as permeability of the cell wall and diffusion properties of CO_2 and HCO_3^- in different components, (b) anatomical parameters such as distance between the cell wall and chloroplast and thickness of the chloroplast, (c) biochemical parameters describing CA activities, and (d) other variables such as environmental CO_2 conditions C_i, net photosynthesis rate A_N, HCO_3^- leakage across the chloroplast envelope lk_b, (photo)respiration rate, and variable φ characterizing the relative position between mitochondria and chloroplasts (Table 1, Spreadsheet **S1**).

To evaluate the robustness of the new model, we first compared its predictions with a 3D R-D model of a rice MSC. Similar responses of r_{liq} to light and CO_2 were predicted by the cell model (Figure 4a) and the analytical model (Figure 4b). The ratio of r_{liq} between the analytical model and cell model was predicted to be around 1.32 under most light and CO_2 conditions. Under low light (150 μmol m^{-2} s^{-1}), this ratio was slightly higher at about 1.4, whereas under low CO_2 (180 μbar), this ratio became approximately 1.2 (Figure 4c). The ratio of C_c between the analytical model and cell model was predicted to be around 0.98 under different light and CO_2 levels (Figure 4d).

Moreover, we evaluated the robustness of the analytical model to predict individual components of r_{liq} by comparing its prediction against those from the 3D cell model. We found that r_{I_wall} calculated from the cell model was almost constant under different light and CO_2 conditions, except under extremely low C_i (Figure 5a). The ratios between r_{I_wall} calculated from the analytical model (Equation 4) and from the cell model were around 0.98 under most light and C_i levels (Figure 5e). Similar levels of deviation were found between predictions of r_{II_cyto} from the analytical model (Equation 5) and the cell model under most conditions (Figure 5b,f). Even under extremely low light, the deviation was still less than 7% (Figure 5f). The deviation of the estimated resistance of the chloroplast envelope (r_{III_se}) between the analytical formula (Equation 8) and the cell model was less than 5% (Figure 5c,g). However, a much higher deviation was observed between the calculated resistance of the stroma (r_{IV_chlo}) between the analytical model and the cell model (Figure 5d,h).

7.2 | Influence of the relative position of mitochondria and chloroplasts on mesophyll conductance

Previously, the g_m–C_i curve simulated using an R-D model of a spherical MSC predicted an increasing trend of g_m with C_i under relatively low C_i followed by a decreasing trend (Tholen & Zhu, 2011), and the initial increase was interpreted as the influence of the (photo)respiratory flux (Tholen et al., 2012; Tholen & Zhu, 2011). However, the CO_2 response of r_{liq} simulated by our cell model showed a monotonic decreasing trend with C_i (Figure 4a). We hypothesized that this

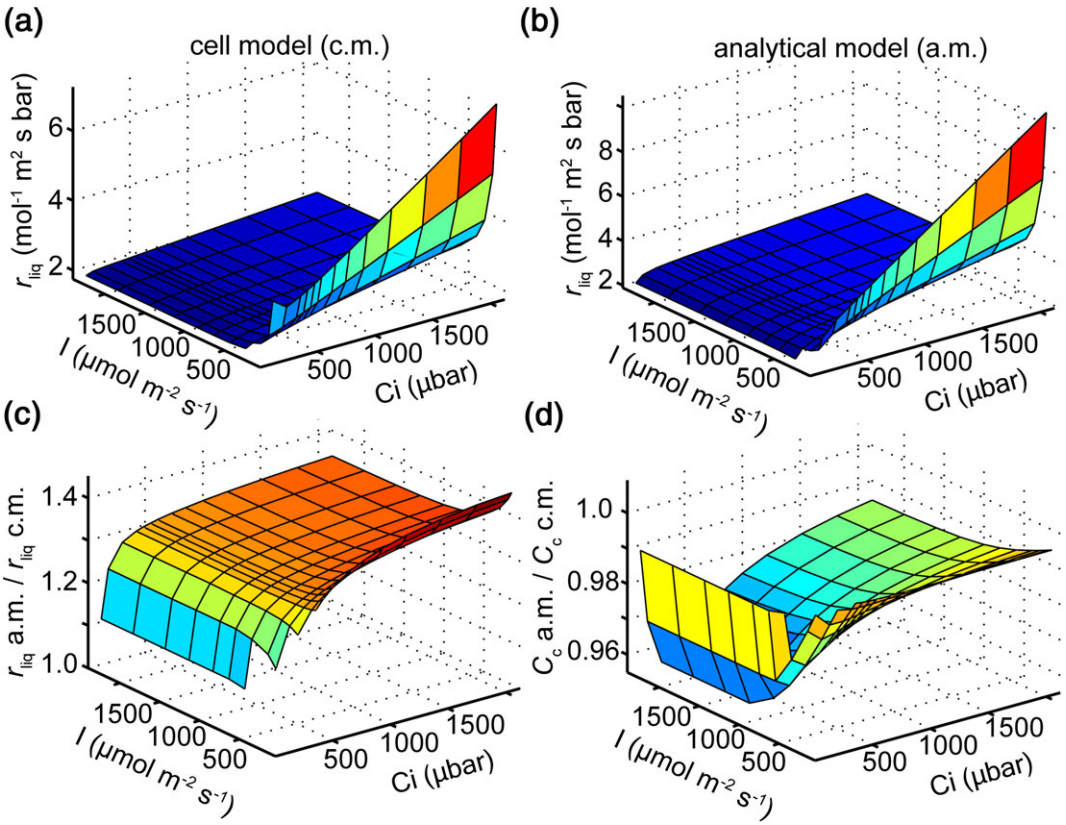

FIGURE 4 The performance evaluation of the new analytical model with a three-dimensional (3D) reaction–diffusion model of rice mesophyll cell in Figure 2b. (a) Liquid-phase mesophyll resistance (r_{liq}) predicted from the 3D cell model under different light and CO_2 conditions. (b) Liquid-phase mesophyll resistance (r_{liq}) predicted from the new analytical model assuming φ equals 0. (c) Ratio of r_{liq} predicted with the analytical model (b) to r_m predicted with the cell model (a). (d) Ratio between the predicted chloroplastic [CO_2] by the analytical model and the cell model under different light and CO_2 levels. I (μmol m^{-2} s^{-1}) in the cell model represents incident irradiance on a leaf surface; absorption of the cell is calculated as average cell absorption in the 3D leaf model

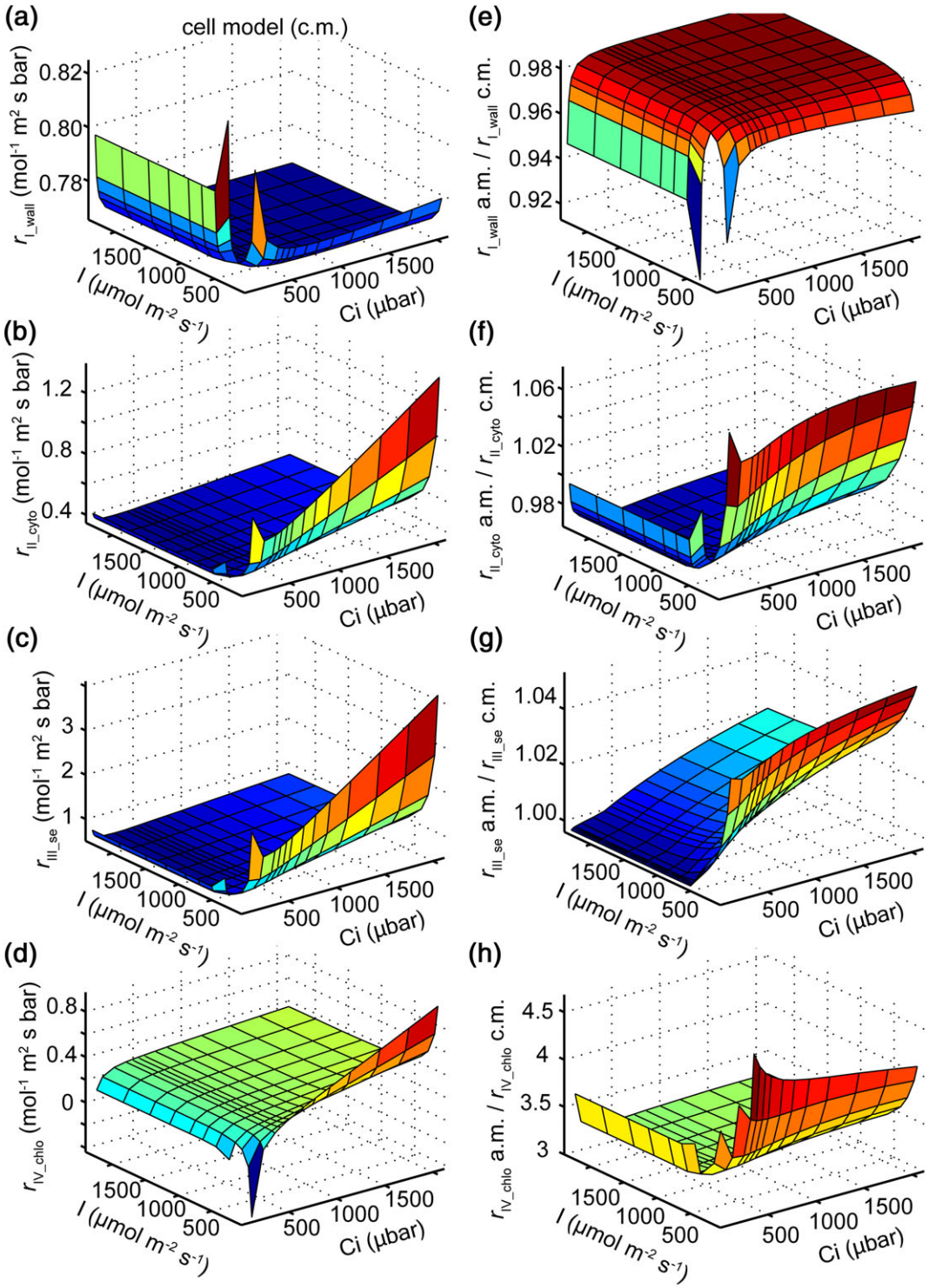

FIGURE 5 (a–d) Resistance of different components of r_{liq} calculated from the three-dimensional reaction–diffusion model under different light and CO_2 conditions. (e–h) Ratio between the resistance of each individual r_{liq} component predicted by the analytical model and three-dimensional cell model corresponding to Panels a–d

difference was because mitochondria in our rice cell model were located completely at the inner side of the chloroplast layer.

To test this hypothesis, we built two types of cell models with four different relative positions between mitochondria and chloroplasts (Figure 3a–d). Simulation shows that the increase of g_{liq} with C_i was directly linked to the location of mitochondria (Figure 6). When mitochondria were totally at the inner side of the chloroplast layer (Figure 3d), the simulated g_{liq}–C_i curve showed a monotonic decreasing trend, similar to the simulated g_{liq}–C_i curve with the default cell model in Figure 2b. When mitochondria were located in the gap between chloroplasts (Figure 3a–c), which was mimicked by holes on the modelled chloroplast membrane layer, the g_{liq}–C_i curve gradually exhibited an increasing trend under low C_i. With a closer distance between mitochondria and the cell wall, the increasing trend became more significant and the C_i value corresponding to the peak in the g_{liq}–C_i curve became larger (Figure 6). In our analytical model, we set

a variable φ to represent this relative location of mitochondria and chloroplasts, which enables the analytical model to predict similar g_{liq}–C_i responses (lower panel in Figure 6) as predicted by 3D cell models (Figure 3 and upper panel in Figure 6).

7.3 | Comparison between the whole mesophyll resistance predicted by the analytical model and three-dimensional leaf model

Scale factor S_m is applied in the analytical formula and the 3D cell model to convert resistances expressed on the basis of exposed cell wall surface area to resistances expressed on the basis of leaf area. This implicitly assumes that the photosynthetic statuses of all MSCs are uniform across the leaf, that is, acting as a single big MSC. However, the light and CO_2 environments inside the leaf are nonuniform (Supporting Information Figures S1 and S2a). With a 3D R-D model of a rice leaf, we also compared the whole r_m predicted by our analytical model and the 3D leaf model. Figure 7a shows the r_m predicted by the leaf model under different light and CO_2 conditions, and Figure 7b shows that the ratio of r_m predicted by the analytical model and the leaf model varies between 1.03 and 1.18 under different light and CO_2 levels. Specifically, Figure 7c shows the calculated r_{ias} by the 3D leaf model. The predicted r_{ias} by the analytical formula (Equation 2) underestimated the value predicted by the leaf model by around 37% (Figure 7d).

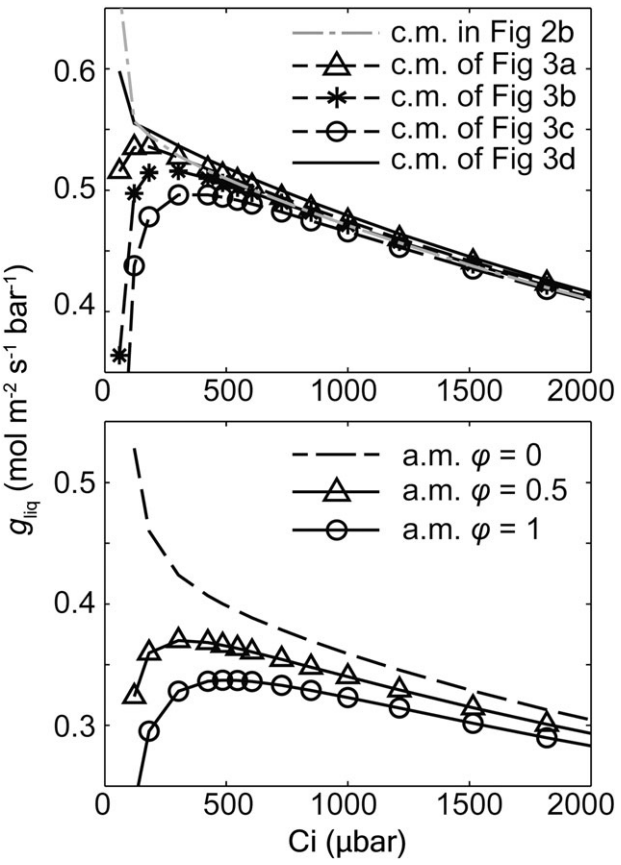

FIGURE 6 Upper panel shows the simulated g_{liq}–C_i curve with different cell anatomies. Black solid line represents the results by anatomy in Figure 3d. Dashed lines with open triangles, stars, and open circles represent the results by anatomy in Figure 3a–c correspondingly. The grey line represents the results predicted by the cell anatomy in Figure 2b. Lower panel shows the predicted g_{liq}–C_i curves from the new analytical model of r_m with different φ; c.m. here is short for the cell model, and a.m. here is short for analytical model

7.4 | Biochemical factors influencing the mesophyll resistance

Mesophyll resistance is analogous to the resistance in Ohm's law. The resistance in electricity is not influenced by either voltage or currency; therefore, it is expected that r_m is not influenced by CO_2 conditions or the photosynthetic rate. We explored the potential biochemical factors leading to this variable r_m under different conditions. Specifically, we sequentially eliminated four potential biochemical factors in the 3D leaf model. First, the effect of nonuniform distribution of light was eliminated by manually assigning the leaf electron transport rate (J) into all chloroplasts uniformly (Figure 8a and Supporting Information Figure S2b). Further, the potential impact of photorespiration and respiration fluxes on r_m was eliminated by setting the Γ^* to be zero so that no CO_2 will be released from the mitochondria (Figure 8b). Moreover, the bicarbonate leakage at the chloroplast envelope was blocked by manually setting the permeability of bicarbonate through the envelope to be zero (Figure 8c). Finally, (de)hydration activities in cytosol and stroma were removed in the R-D equation (Figure 8d). The corresponding r_m of each model under different light and CO_2 levels was predicted. We found that these four factors all contributed to the variation of r_m under different light and CO_2 conditions. When all these different biochemical components were eliminated, we obtained a constant r_m under different light and relatively high CO_2 levels (Figure 8d). Under this situation, there are only CO_2 diffusion and carboxylation in the 3D leaf. When the leaf was not CO_2 saturated, an increase of r_m with C_i was still observed due to the change of effective path length under the 3D nature of diffusion (Figure 8d).

8 | DISCUSSION

8.1 | A new analytical formula representing mesophyll resistance as a property of a complex biophysical, biochemical, and anatomical system

Mesophyll resistance (r_m) is an integrative leaf parameter jointly controlled by a large array of complex biophysical, biochemical, and 3D anatomical factors. Tholen et al. (2012) developed an analytical model of r_m, which incorporated the effects of (photo)respiratory fluxes. A number of studies have measured anatomical features and r_m of different species and used them to parameterize r_m models (Berghuijs et al., 2015; Peguero-Pina et al., 2012; Tomás et al., 2013; Tosens et al., 2012). In these models, resistances of different barriers (cell wall, cytosol, chloroplast envelope, and chloroplast stroma) were calculated based on (a) the measured thickness of the cell wall, cytosol, and chloroplast and (b) assumptions about diffusive properties such as effective diffusive path length, porosity, and viscosity (Tomás et al., 2013). Recently, Berghuijs et al. (2015) combined the frameworks of Tholen et al. and Tomás et al. (2013) to produce a new r_m model, with which the impacts of (photo)respiratory flux and leaf anatomical factors on r_m can be explored.

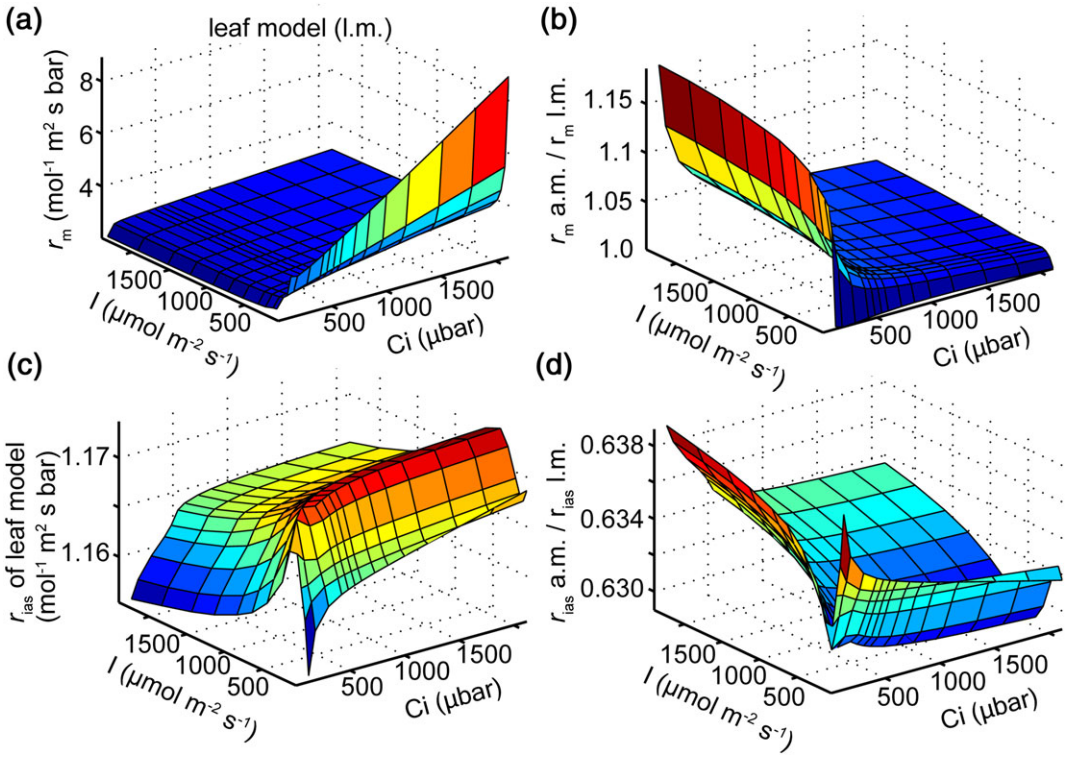

FIGURE 7 The performance evaluation of the new analytical model with a three-dimensional (3D) reaction–diffusion model of rice leaf in Figure 2 b. (a) Total r_m predicted from the 3D leaf model. (b) The ratio of r_m predicted with the analytical model (a.m.) to r_m predicted with the leaf model under different light and CO_2 conditions. (c) Gaseous-phase mesophyll resistance (r_{ias}) predicted from the 3D leaf model. (d) The ratio of r_{ias} predicted by a.m. and leaf model under different light and CO_2 conditions

Here, with a mechanistic 3D R-D model to set as the ground truth, we developed a new analytical formula of r_m, which explicitly incorporates all known anatomical and biochemical components of r_m. Values set in the 3D R-D model such as porosity, viscosity, Γ^*, and R_d can be directly used in the analytical formula, which enables us to directly evaluate the accuracy of analytical models to predict not only the whole leaf r_m but also its components. Here, we compare the prediction from our new analytical model with earlier r_m model predictions by Tomás et al. (2013) and Tholen et al. (2012). The formula of resistance of intercellular air space (r_{ias}, Equation 2) and the formula of resistance of the cell wall and plasma membrane (r_{l_wall}, Equation 4) are the same between our new model and the model by Tomás et al. Compared to r_{ias} predicted from the 3D leaf model, r_{ias} was underestimated by this formula (Figure 7d), which suggests that the accuracy of this formula may be influenced by different structures of intercellular air space. In other words, tortuosity under different leaf anatomies needs to be incorporated later into this formula, as suggested by Parkhurst (1994).

For the resistance of cytosol, Tomás et al. (2013) predicted a resistance equal to 0.6 mol^{-1} m^{-2} s bar without considering the hydration process. Our formula (Equation 5), which explicitly considers the hydration process, predicted that under a C_i of 30 μbar and a photosynthetic photon flux density of 800 μmol m^{-2} s^{-1}, the total cytosolic resistance (r_{II_cyto}) was 0.34 mol^{-1} m^{-2} s bar (Figure 5b,f), whereas among this, the resistance due to limitation from hydration catalysed by CA ($r_{II\_cyto\_CA}$) was 0.26 mol^{-1} m^{-2} s bar (76% of r_{II_cyto}). Therefore, although the facilitation of CO_2 diffusion by hydration decreased the resistance of cytosol significantly, the hydration rate catalysed by CA also contributed to r_{II_cyto} substantially, which was earlier attributed to the nonequilibrium status of the hydration reaction in cytosol (Tholen & Zhu, 2011). For the resistance of the chloroplast envelope, Tomás et al. calculated it to be 0.39 mol^{-1} m^{-2} s bar, whereas our analytical formula (Equation 8) and 3D cell model predicted this resistance to be mostly around 0.5 to 0.8 mol^{-1} m^{-2} s bar under various conditions (Figure 5c,g). This difference between predictions using our new analytical model and the Tomás et al. model is caused by the HCO_3^- efflux on the chloroplast envelope in our analytical formula. Theoretically, this leakage of HCO_3^- will be influenced by pH, [CO_2], activity of CA in the cytosol and stroma, and the permeability of the envelope to HCO_3^- (Tholen & Zhu, 2011). Our new analytical model provides an opportunity to explore these different factors.

For the resistance of the stroma (r_{IV_chlo}), Tomás et al. (2013) calculated it to be as high as 7.56 mol^{-1} m^{-2} s bar, which is equal to the ratio between half the chloroplast thickness and CO_2 diffusion coefficient in the stroma. However, the r_{IV_chlo} predicted from our 3D cell model was mostly less than 0.5 mol^{-1} m^{-2} s bar (Figure 5d). This much lower r_{IV_chlo} is attributed to two factors: (a) the facilitated diffusion by CA and (b) carboxylation occurring throughout the stroma instead of being at the midpoint of the stroma as assumed by Tomás et al. Our analytical formula considers the effect of hydration; therefore, the relative error for r_{IV_chlo} is smaller but still as high as around 200% (Figure 5h), which is the main reason leading to the relative error of 32% for the total r_{liq} (Figure 4c). Two factors contributed to this high relative error. First, as a result of the diffusion into an ever-decreasing volume inside a 3D chloroplast, the concentration and fluxes of CO_2

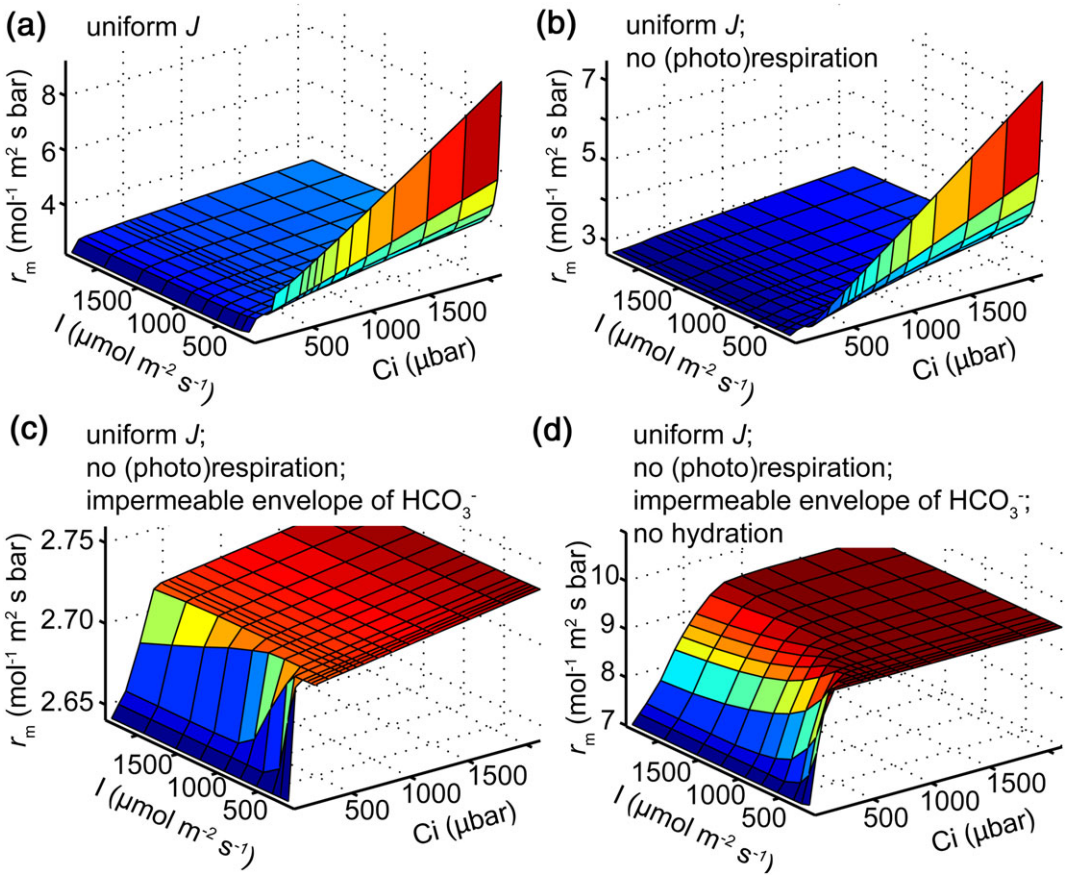

FIGURE 8 The mesophyll resistance (r_m) predicted by four different three-dimensional reaction–diffusion leaf models, in which different biochemical factors influencing r_m are eliminated sequentially. These four models are as follows: (a) same model as the default leaf model in Figure 7a except that the effective electron transport rate was manually assigned uniformly inside all the chloroplasts; (b) same model as in Panel a except that the (photo)respiration was eliminated; (c) same model as in Panel b except that the chloroplast envelope was set to be impermeable to the bicarbonate; (d) same model as in Panel c except that the hydration process in the cytosol and chloroplast was blocked so that only CO_2 diffusion and carboxylation remained

and HCO_3^- on a unit volume basis gradually increase with depth into the chloroplast. This is analogous to the situation when CO_2 diffuses from the stomata to intercellular air space, which is essentially diffusion in an ever-increasing volume in 3D (Parkhurst, 1994). This 3D nature of diffusion is ignored in the analytical model. Second, r_{IV_chlo} is calculated as the ratio of C_{se_i}–C_c and net photosynthesis rate, where C_c is an average value of $[CO_2]$ in the whole stroma and C_{se_i} is the $[CO_2]$ in the inner boundary of the chloroplast envelope. An accurate estimate of C_c requires an accurate prediction of the distribution of $[CO_2]$ in the stroma, which is difficult to achieve in the 1D analytical model. Furthermore, because r_{IV_chlo} is the last component of the r_m, C_c is numerically close to C_{se_i} in the R-D model, and the difference between C_c and C_{se_i} is very small; as a result, even a 3% deviation in the calculated C_c between the analytical model and 3D cell model can generate an over 200% deviation in the calculated r_{IV_chlo}, as compared to the 3D cell model.

Tholen et al. (2012) developed Equation 10 to account for the effect of (photo)respiration on r_m under different CO_2 conditions,

$$r_m = r_w + r_{ch}\frac{A_N + F + R_d}{A_N}, \tag{10}$$

where r_w represents the resistance of the cell wall and plasma membrane and r_{ch} represents the resistance of chloroplast envelope and stroma. An equivalent form of r_{liq} in our analytical model (Equation 3) is written as follows:

$$r_{liq} = (r_{I\_wall} + r_{II\_cyto}) + \left(\frac{C_{se\_o} - C_c}{F_x}\right)\frac{F_x}{A_N}, \tag{11}$$

where F_x equals $A_N + \varphi(F + R_d)$. The F_x is used here to make the flux on the denominator correspond to the CO_2 gradient on the numerator. To degenerate from our analytical model (Equation 11) to Tholen's model (Equation 10), three conditions need to be satisfied: (a) r_{II_cyto} is much less than r_{I_wall} in Equation 11; (b) F_x equals $A_N + F + R_d$, which means φ in our analytical model is 1; (c) $C_{se\_o} - C_c/F_x$ equals a constant r_{ch}, which means the influence of carboxylation, hydration, and bicarbonate leakage to resistance of the chloroplast envelope and stroma is negligible (Equations 8 and 9); thus, $C_{se\_o} - C_c/F_x$ approximates a constant. This third simplification makes Tholen's model (Equation 10) unable to predict the decreasing trend of g_m at high C_i. Both our analytical model and the 3D R-D models in this study (Figure 6) and of Tholen and Zhu (2011) can predict this decreasing trend.

During the deduction of our analytical model, the fluxes A_N, $F + R_d$, and lk_b were preserved in the formula of r_{II_cyto}, r_{III_se}, and r_{IV_chlo} (Equations 5, 8, and 9), and those fluxes cannot be eliminated like C_{w_i}, C_{se_o}, and C_{se_i}. Essentially, it is because r_m is a parameter defined on an indivisible complex system. Although it seems that we can divide the r_{liq}

into four components by Equation 3, any changes in the resistance of one barrier would affect the resistances of the other three barriers. This coupling between different components of r_m is manifested through fluxes A_N, $F + R_d$, and lk_b in the analytical model.

8.2 | Practical considerations during the application of the new analytical model

Comparison studies show that our analytical model can predict the r_m with a high level of accuracy (Figure 5). However, during applications on real leaf, the calculated r_m using the analytical model can potentially deviate from the r_m experimentally measured due to a number of reasons. First, the formulas of r_{l_wall} may still possibly deviate, although it seems to have a very high accuracy compared with the 3D model (Figure 5e), as effective porosity of the cell wall in the formula of r_{l_wall} may vary between different species. Different leaves have different structures of intercellular air space, which also affects the accuracy of the formula of r_{ias} without changing the tortuosity.

Second, during the application of our analytical model (Spreadsheet **S1**), A_N and $F + R_d$ per leaf area can be experimentally measured. So far however there is no method developed for the measurement of lk_b. In this study, we estimated lk_b under different light and CO_2 levels from the 3D R-D models. Then the estimated lk_b was applied in the analytical model to correct the effect of bicarbonate leakage to r_m. Simulations with our leaf model show that the ratio of lk_b to A was around 0.27 to 3 under most light and CO_2 conditions in our model (Supporting Information Figure S3). Under ambient CO_2 and relative high light (e.g., photosynthetic photon flux density > 400 μmol m^{-2} s^{-1}), this ratio was predicted to be between 0.27 and 0.54 (data attached in Spreadsheet **S1**). This ratio can potentially be different under different CA concentrations and pH in cytosol and stroma, which is at this point not considered in the current analytical model. More work is needed still to measure lk_b to better use our analytical approach.

Furthermore, the factor φ in our analytical model, which represents the effect of relative special location between mitochondria and chloroplast on r_m, is also difficult to estimate directly from the anatomical measurements of leaf. For plants such as rice, which has a very high chloroplast coverage, we can approximate φ to be 0. However, for other leaf anatomies, the best way to infer φ is possibly through numerical estimation based on sophisticated 3D modelling. Especially for leaf with a low chloroplast coverage, the r_m is influenced not only by the scale factor S_c but also because of the effect of φ. Moreover, it is worth noting that the value of φ is not necessarily a constant under different light and CO_2 conditions, considering the relative changes in A_N and $F + R_d$ with the change of environmental conditions.

In Table 2, we list all these contributing factors that can potentially decrease the accuracy of the analytical model and hence are potential areas of future research. Briefly, deviation between r_m calculated by our analytical model and r_m measured on a real leaf is introduced during three steps, that is, during simplification of the 3D cell model to the analytical model, during simplification of a 3D leaf model to a 3D cell model, and during representation of a real leaf into a 3D leaf model.

TABLE 2 Potential mechanisms leading to the difference of mesophyll resistance between a real leaf, a three-dimensional (3D) leaf model, and a 3D cell model

Scopes	Potential errors that affect mesophyll resistance
Real leaf versus 3D leaf model	Deviations made in experimental measurement of gas exchange, chlorophyll *a* fluorescence, and carbon isotope discrimination Representative modelled leaf anatomy Assumed parameters difficult to measure in the model (porosity of the wall and membrane, diffusive viscosity, etc.) Simplifications made during the modelling process Factors not modelled and beyond our current knowledge
3D leaf model versus 3D cell model	Representative cell anatomy; estimation of S_m/S Nonuniform photosynthesis inside the leaf Resistance of the gaseous phase in different 3D leaf anatomies
3D cell model versus analytical model	3D nature of diffusion and one-dimensional approximation Accuracy of the form of the analytical model Accuracy of the input parameters of the analytical model Chloroplast arrangement and mitochondria position; parameter of φ

8.3 | Does photorespiration and respiration influence the mesophyll resistance?

Tholen and Zhu (2011, 2012) suggested that photorespiration and respiration led to the intrinsic decrease of r_m under low C_i. Evans and von Caemmerer (2013) measured the response of $\Delta^{13}C$ signal to oxygen concentration and observed that fractionation of photorespiration (Δ_f) responded in a linear way to the oxygen concentration; therefore, they suggested a higher factor f (fractionation factor of photorespiration) to explain the decrease of r_m under low C_i. Evans and von Caemmerer (2013) explained the results of Tholen et al. (2012) by artefacts with the equation of $\Delta^{13}C$ signal and biased f used in the data analysis (Griffiths & Helliker, 2013). However, due to the unknown real value of f, we still cannot rule out the possibility that (photo)respiration influences r_m. In other words, (photo)respiration may still affect the intrinsic r_m and then affect the measured r_m by the $\Delta^{13}C$ method. Meanwhile, it may also affect the factor f therefore involved in the interpretation of the $\Delta^{13}C$ signal and the calculated r_m (Griffiths & Helliker, 2013).

In our simulation, we showed that the position of mitochondria affected the response of r_m with C_i (Figures 3 and 6), and a factor φ was introduced to represent this effect, which means only part of the (photo)respiratory flux, $\varphi(F + R_d)$, influenced the CO_2 flux between the cell wall and chloroplast. In this sense, theoretically, φ would influence both the value of f and the degree of the effect of (photo)respiration on r_m. The interaction between the position of mitochondria, f, and the (photo)respiratory flux was not considered in previous experiments and simulations. A new model of the R-D process of $^{13}CO_2/^{12}CO_2$ in the future can potentially form a unified theoretical framework to simulate the measured $\Delta^{13}C$ signal and to disentangle the mechanism(s) contributing to the variation of r_m under different environments.

9 | CONCLUSION

This study develops a set of models that can be used together to dissect anatomical and biochemical factors controlling mesophyll resistance (r_m), one of the most important parameter controlling photosynthetic efficiency. The new 3D model, which incorporates light propagation and CO_2 R-D processes in a leaf, can be used to study the effects of manipulating each individual biochemical, biophysical, and anatomical leaf features on r_m. With this model, we showed that nonuniform light distribution, (photo)respiration, bicarbonate leakage on the chloroplast envelope, hydration process, and anatomical features can influence r_m and hence can be potential targets to manipulate for improved r_m. We then focus on one 3D cell from the 3D leaf model and found that the relative position of mitochondria with chloroplast greatly influence r_m. Using the predictions from this one 3D cell as ground truth, we derived a comprehensive biochemical–biophysical–anatomical formula of mesophyll resistance incorporating all these identified factors. The new analytical model shows a reliable accuracy in predicting the resistance of different barriers and the chloroplastic CO_2 concentration and provides a relatively easy-to-use tool to evaluate the effects of these different factors on r_m for a particular leaf. The identified factors related to r_m and the models developed here will not only facilitate future mechanistic study of r_m but also support current effort of engineering r_m for improved photosynthesis.

ACKNOWLEDGEMENTS

The authors would like to thank Tom Sharkey and two anonymous reviewers for their constructive comments and Danny Tholen for his helpful comments and discussions on the manuscript. Funding for authors' research is from the Bill and Melinda Gates Foundation (grants OPP1014417, OPP1060461, and OPP1129902), the Chinese Academy of Sciences (XDA08020301), National Science Foundation of China (grant 30970213), Ministry of Science and Technology of China (grants 2011DFA and 2015CB150104).

ORCID

Xin-Guang Zhu http://orcid.org/0000-0002-4435-130X

REFERENCES

Berghuijs, H. N. C., Yin, X., Tri, H. Q., van der Putten, P. E. L., Verboven, P., Retta, M. A., … Struik, P. C. (2015). Modeling the relationship between CO_2 assimilation and leaf anatomical properties in tomato leaves. *Plant Science*, *238*, 297–311.

Busch, F. A., Sage, T. L., Cousins, A. B., & Sage, R. F. (2013). C_3 plants enhance rates of photosynthesis by reassimilating photorespired and respired CO_2. *Plant, Cell & Environment*, *36*, 200–212.

Douthe, C., Dreyer, E., Brendel, O., & Warren, C. R. (2012). Is mesophyll conductance to CO_2 in leaves of three *Eucalyptus* species sensitive to short-term changes of irradiance under ambient as well as low O_2? *Functional Plant Biology*, *39*, 435–448.

Douthe, C., Dreyer, E., Epron, D., & Warren, C. R. (2011). Mesophyll conductance to CO_2, assessed from online TDL-AS records of $^{13}CO_2$ discrimination, displays small but significant short-term responses to CO_2 and irradiance in *Eucalyptus* seedlings. *Journal of Experimental Botany*, *62*, 5335–5346.

Evans, J. R. (2009). Potential errors in electron transport rates calculated from chlorophyll fluorescence as revealed by a multilayer leaf model. *Plant & Cell Physiology*, *50*, 698–706.

Evans, J. R., Kaldenhoff, R., Genty, B., & Terashima, I. (2009). Resistances along the CO_2 diffusion pathway inside leaves. *Journal of Experimental Botany*, *60*, 2235–2248.

Evans, J. R., & von Caemmerer, S. (2013). Temperature response of carbon isotope discrimination and mesophyll conductance in tobacco. *Plant, Cell & Environment*, *36*, 745–756.

Farquhar, G. D., & Cernusak, L. A. (2012). Ternary effects on the gas exchange of isotopologues of carbon dioxide. *Plant, Cell & Environment*, *35*, 1221–1231.

Flexas, J., Barbour, M. M., Brendel, O., Cabrera, H. M., Carriquí, M., Díaz-Espejo, A., … Warren, C. R. (2012). Mesophyll diffusion conductance to CO_2: An unappreciated central player in photosynthesis. *Plant Science*, *193–194*, 70–84.

Flexas, J., Diaz-Espejo, A., Galmés, J., Kaldenhoff, R., Medrano, H., & Ribas-Carbo, M. (2007). Rapid variations of mesophyll conductance in response to changes in CO_2 concentration around leaves. *Plant, Cell & Environment*, *30*, 1284–1298.

Griffiths, H., & Helliker, B. R. (2013). Mesophyll conductance: Internal insights of leaf carbon exchange. *Plant, Cell & Environment*, *36*, 733–735.

Gu, L., & Sun, Y. (2014). Artefactual responses of mesophyll conductance to CO_2 and irradiance estimated with the variable J and online isotope discrimination methods. *Plant, Cell & Environment*, *37*, 1231–1249.

Gu, J., Yin, X., Stomph, T.-J., Wang, H., & Struik, P. C. (2012). Physiological basis of genetic variation in leaf photosynthesis among rice (*Oryza sativa* L.) introgression lines under drought and well-watered conditions. *Journal of Experimental Botany*, *63*, 5137.

Harley, P. C., Loreto, F., Di Marco, G., & Sharkey, T. D. (1992). Theoretical considerations when estimating the mesophyll conductance to CO_2 flux by analysis of the response of photosynthesis to CO_2. *Plant Physiology*, *98*, 1429–1436.

Hassiotou, F., Ludwig, M., Renton, M., Veneklaas, E. J., & Evans, J. R. (2009). Influence of leaf dry mass per area, CO_2, and irradiance on mesophyll conductance in sclerophylls. *Journal of Experimental Botany*, *60*, 2303–2314.

Loriaux, S. D., Avenson, T. J., Welles, J. M., Mcdermitt, D. K., Eckles, R. D., Riensche, B., & Genty, B. (2013). Closing in on maximum yield of chlorophyll fluorescence using a single multiphase flash of sub-saturating intensity. *Plant, Cell & Environment*, *36*, 1755–1770.

Niinemets, Ü., & Reichstein, M. (2003). Controls on the emission of plant volatiles through stomata: A sensitivity analysis. *Journal of Geophysical Research: Atmospheres*, *108*, 4211.

Nobel, P. S. (1999). *Physicochemical and environmental plant physiology*. San Diego: Academic Press.<!---->

Parkhurst, D. F. (1994). Diffusion of CO_2 and other gases inside leaves. *New Phytologist*, *126*, 449–479.

Peguero-Pina, J. J., Flexas, J., Galmés, J., Niinemets, Ü., Sancho-Knapik, D., Barredo, G., … Gil-Pelegrín, E. (2012). Leaf anatomical properties in relation to differences in mesophyll conductance to CO_2 and photosynthesis in two related Mediterranean *Abies* species. *Plant, Cell & Environment*, *35*, 2121–2129.

Pons, T. L., Flexas, J., von Caemmerer, S., Evans, J. R., Genty, B., Ribas-Carbo, M., & Brugnoli, E. (2009). Estimating mesophyll conductance to CO_2: Methodology, potential errors, and recommendations. *Journal of Experimental Botany*, *60*, 2217–2234.

Sage, T. L., & Sage, R. F. (2009). The functional anatomy of rice leaves: Implications for refixation of photorespiratory CO_2 and efforts to engineer C_4 photosynthesis into rice. *Plant & Cell Physiology*, *50*, 756–772.

Tazoe, Y., von Caemmerer, S., Badger, M. R., & Evans, J. R. (2009). Light and CO_2 do not affect the mesophyll conductance to CO_2 diffusion in wheat leaves. *Journal of Experimental Botany*, *60*, 2291–2301.

Tazoe, Y., von Caemmerer, S., Estavillo, G. M., & Evans, J. R. (2011). Using tunable diode laser spectroscopy to measure carbon isotope discrimination and mesophyll conductance to CO_2 diffusion dynamically at different CO_2 concentrations. *Plant, Cell & Environment*, *34*, 580–591.

Théroux-Rancourt, G., & Gilbert, M. E. (2017). The light response of mesophyll conductance is controlled by structure across leaf profiles. *Plant, Cell & Environment*, *40*, 726–740.

Tholen, D., Éthier, G., & Genty, B. (2014). Mesophyll conductance with a twist. *Plant, Cell & Environment*, *37*, 2456–2458.

Tholen, D., Éthier, G., Genty, B., Pepin, S., & Zhu, X.-G. (2012). Variable mesophyll conductance revisited: Theoretical background and experimental implications. *Plant, Cell & Environment*, *35*, 2087–2103.

Tholen, D., & Zhu, X.-G. (2011). The mechanistic basis of internal conductance: A theoretical analysis of mesophyll cell photosynthesis and CO_2 diffusion. *Plant Physiology*, *156*, 90–105.

Tomás, M., Flexas, J., Copolovici, L., Galmés, J., Hallik, L., Medrano, H., … Niinemets, Ü. (2013). Importance of leaf anatomy in determining mesophyll diffusion conductance to CO_2 across species: Quantitative limitations and scaling up by models. *Journal of Experimental Botany*, *64*, 2269–2281.

Tosens, T., & Niinemets, U. (2012). Developmental changes in mesophyll diffusion conductance and photosynthetic capacity under different light and water availabilities in *Populus tremula*: How structure constrains function. *Plant, Cell & Environment*, *35*, 839–856.

Tosens, T., Niinemets, Ü., Westoby, M., & Wright, I. J. (2012). Anatomical basis of variation in mesophyll resistance in eastern Australian sclerophylls: News of a long and winding path. *Journal of Experimental Botany*, *63*, 5105–5119.

Vrábl, D., Vašková, M., Hronková, M., Flexas, J., & Šantrček, J. (2009). Mesophyll conductance to CO_2 transport estimated by two independent methods: Effect of variable CO_2 concentration and abscisic acid. *Journal of Experimental Botany*, *60*, 2315–2323.

Xiao, Y., Tholen, D., & Zhu, X.-G. (2016). The influence of leaf anatomy on the internal light environment and photosynthetic electron transport rate: Exploration with a new leaf ray tracing model. *Journal of Experimental Botany*, *67*, 6021–6035.

Xiong, D., Liu, X., Liu, L., Douthe, C., Li, Y., Peng, S., & Huang, J. (2015). Rapid responses of mesophyll conductance to changes of CO_2 concentration, temperature and irradiance are affected by N supplements in rice. *Plant, Cell & Environment*, *38*, 2541–2550.

Zhu, X.-G., Long, S. P., & Ort, D. R. (2010). Improving photosynthetic efficiency for greater yield. *Annual Review of Plant Biology*, *61*, 235–261.

SUPPORTING INFORMATION

Additional Supporting Information may be found online in the supporting information tab for this article.

How to cite this article: Xiao Y, Zhu X-G. Components of mesophyll resistance and their environmental responses: A theoretical modelling analysis. *Plant Cell Environ.* 2017;40:2729–2742. https://doi.org/10.1111/pce.13040